Astrophys Space Sci (2009) 321: 109–122
DOI 10.1007/s10509-009-0014-x

ORIGINAL ARTICLE

Study of accretion disk dynamics in presence of cooling

Santabrata Das · Chul-Sung Choi

Received: 11 December 2008 / Accepted: 18 February 2009 / Published online: 4 March 2009

Abstract We examine the behaviour of accretion flow around a rotating black hole in presence of cooling. We obtain global flow solutions for various accretion parameters that govern the accreting flow. We show that standing isothermal shock wave may develop in such an advective accretion flow in presence of cooling. This shocked solution has observational consequences as it successfully provides the possible explanations of energy spectra as well as generation of outflows/jets of various galactic and extra-galactic black hole candidates. We study the properties of isothermal shock wave and find that it strongly depends on the cooling efficiency. We identify the region in the parameter space spanned by the specific energy and specific angular momentum of the flow for standing isothermal shock as a function of cooling efficiencies and find that parameter space gradually shrinks with the increase of cooling rates. Our results imply that accretion flow ceases to contain isothermal shocks when cooling is beyond its critical value.

Keywords Accretion · Accretion disc · Black hole physics · Shock waves

1 Introduction

Fluid dynamical studies of advective accretion disks around black holes has been performed extensively as a model of many astrophysical system including active galactic nuclei, quasars and microquasars (Abramowicz et al. 1988; Chakrabarti 1990, 1996a, 1996b; Narayan and Yi 1994; Yang and Kafatos 1995; Manmoto 2000; Becker and Le 2003). This disk model successfully provides a possible explanation of emission properties of black hole candidates as a result of their high temperature (Chakrabarti and Titarchuk 1995; Hameury et al. 1997; Chakrabarti and Mandal 2006). The characteristic feature of such an accretion process around the black holes is that the solution must be globally transonic as flow has to cross the event horizon supersonically in order to fulfill the inner boundary conditions enforced by the black hole. Numerical simulation of advective accretion flow reveals that rotating inflowing matter feels a barrier due to centrifugal pressure that stimulates the flow to transit through the shock (Hawley et al. 1984a, 1984b; Chakrabarti and Molteni 1993). Furthermore, analytical calculation also confirms the existence of standing shocks that are radiatively quite inefficient (Rankine-Hugoniot shocks) (Das et al. 2001a). The global flow solution, with or without shock, can be determined by the fundamental accretion parameters namely, energy and angular momentum of the flow at a large distance. It has been speculated by a number of authors that shocked accretion flow might have natural prospectus for explaining the spectral properties and launching the outflows/jets as frequently observed in many accretion system (Chakrabarti and Titarchuk 1995; Chakrabarti 1999; Das et al. 2001b; Le and Becker 2005; Chakrabarti and Mandal 2006; Chattopadhyay and Das 2007; Fukumura and Kazanas 2007; Das and Chattopadhyay 2008).

The basic thermodynamical properties of hydrodynamic accretion flow are extensively examined for a various group of workers in both non-dissipative (Fukue 1987;

S. Das (✉) · C.-S. Choi
International Center for Astrophysics, Korea Astronomy and Space Science Institute, 61-1, Hwaam Dong, Yuseong-Gu, Daejeon 305 348, South Korea
e-mail: sbdas@canopus.cnu.ac.kr

C.-S. Choi
e-mail: cschoi@kasi.re.kr

Chakrabarti 1990; Fukumura and Tsuruta 2004) and viscous flows (Chakrabarti 1996b; Chakrabarti and Das 2004) considering Rankine-Hugoniot shock conditions. Very recently, stationary shock waves in magnetohydrodynamic accretion flow is also studied for a wide range of accretion parameters (Das and Chakrabarti 2007 and references therein). Actually, Rankine-Hugoniot shock transition is observed in an extreme physical conditions where shock is treated as radiatively inefficient as energy of the flow across the shock remains uniform. In the other extreme, accreting matter may encounter isothermal shock transition where excess flow energy is efficiently radiated away through the disk surface to maintain uniform temperature distribution across the shock. This preserves the regular disk structure just before and just after the shock. In an earlier attempt, (Chakrabarti and Abramowicz 1990) presented a systematic studies of isothermal shock waves for an adiabatic flow. Later, Lu and Yuan (1998) and Fukumura and Tsuruta (2004) discussed the issue of existence of isothermal shocks considering full general relativity for adiabatic flow. Das et al. (2003) also studied isothermal shocks in the isothermal flow using various Pseudo-potentials for Schwarzschild black hole. In all these works, it was reported that isothermal shock location behaves as a natural site of radiation source that may be responsible to power the observed X-ray flares (Miller 2007). In addition, (Becker and Le 2003; Le and Becker 2005) estimated the power of the relativistic outflows that are being ejected at the location of the isothermal shock. However, all the above mentioned efforts was made either in the limit of adiabatic or isothermal approximations. In the present work, we wish to study stationary, axisymmetric, dissipative accretion flow around a rotating black hole. In particular, we address the issue of isothermal shock formation considering synchrotron cooling. We adopt pseudo-Kerr potential that satisfactorily describe the space-time geometry around a rotating black hole. We provide the dependence of all the relevant dynamical and thermodynamical flow variables on the fundamental accretion parameters. We study the requisite accretion flow solution that may allow isothermal shock transition. In this work, shock location is virtually acts as a boundary layer to the accreting matter where huge amount of luminosity ($\sim 10^{37} \frac{M_{BH}}{M_\odot}$ ergs sec^{-1}) is released. Thus, shocks under consideration are very bright and it may play an important role as it dominates the high-energy radiation over the entire accretion system. Thus, isothermal shock has a profound observational consequences and therefore, it is important to explore the effect of cooling process on the properties of isothermal shock, specially how the dynamics of these discontinuities is controlled by the dissipation since cooling has a significant effect on the disk structure.

The structure of the paper is organized as follows. In the Sect. 2, we present the basic equations for the present purpose. Accretion flow solutions are discussed in Sect. 3. The main results are discussed in Sect. 4. We identify the parameter space for stationary isothermal shocks in Sect. 4. Finally, in Sect. 5, we present concluding remarks.

2 Models and assumptions

We consider a rotating gas that is accreted on to a rotating black hole of mass M_{BH} and obey the polytropic equation of state. Furthermore, the flow is assumed to be steady, axisymmetric and viscous. Flow variables are averaged in the vertical direction. The effect of gravity is taken care by the pseudo-Kerr potential introduced by (Mondal and Chakrabarti 2006). The self-gravity of the accreting matter is ignored. Cylindrical coordinates (x, ϕ, z) is adopted with the z-axis being the rotation axis of the disk. In this paper, we choose units of distance, velocity and angular momentum to be GM_{BH}/c^2, c and GM_{BH}/c respectively, where, G and c are the gravitational constant and speed of light.

2.1 Basic equations

The stationary mass accretion rate is obtained from the equation of continuity which is given by,

$$\dot{M} = 4\pi u \Sigma x, \tag{1}$$

where, u, Σ and $\dot{M}$ are the radial velocity, vertically averaged density and the mass accretion rate respectively.

In the steady state, the equation of motion in radial and azimuthal directions are written down in the disk equatorial plane as:

$$u\frac{du}{dx} + \frac{1}{\rho}\frac{dP}{dx} + \frac{d\Phi_e}{dx} = 0, \tag{2}$$

and

$$u\frac{d\lambda}{dx} + \frac{1}{\Sigma x}\frac{d}{dx}\left(x^2 W_{x\phi}\right) = 0, \tag{3}$$

where, ρ, P, λ, and $W_{x\phi}$ are the density, isotropic pressure, specific angular momentum and viscous stress of the flow respectively. The third term of (2) is the derivative of the effective potential calculated at the disk equatorial plane. The expression of pseudo-Kerr effective potential is given by,

$$\Phi = -\frac{\Phi_2 + \sqrt{\Phi_2^2 - 4\Phi_1\Phi_3}}{2\Phi_1},$$

where,

$$\Phi_1 = \frac{\alpha^2\lambda^2}{2x^2}, \quad \Phi_2 = -1 + \frac{\alpha^2\omega\lambda R^2}{x^2} + \frac{2a_k\lambda}{R^2 x}$$

and $$\Phi_3 = 1 - \frac{1}{R - x_0} + \frac{2a_k\omega}{x} + \frac{\alpha^2\omega^2 R^4}{2x^2}.$$

Here, R represents the radial coordinate and x denotes the projection distance of R along the disk equatorial plane from the black hole when the black hole itself is considered to be located at the origin of the cylindrical coordinate system. Furthermore, $x_0 = (0.04 + 0.97a_k + 0.085a_k^2)/2$, $\omega = 2a_k/(x^3 + a_k^2 x + 2a_k^2)$ and $\alpha^2 = (x^2 - 2x + a_k^2)/(x^2 + a_k^2 + 2a_k^2/x)$, α is the red shift factor. Black hole rotation parameter is defined as the specific spin angular momentum and denoted by a_k. The subscripts 'e' stands for the quantities calculated at the disk equatorial plane.

The energy equation for accreting flow is expressed as,

$$\Sigma u T \frac{ds}{dx} = Q^+ - Q^-, \tag{4}$$

where, s, T, Q^+ and Q^- represent the specific entropy, the local flow temperature, heating and radiative cooling rate, respectively. In the present work, the accreting flow is assumed to be in hydrostatic equilibrium in the vertical direction of the flow motion. The half scale height (h) of the disc estimated (Matsumoto et al. 1984) as,

$$h(x) = a\sqrt{\frac{x}{\gamma \Phi'_R}},$$

where, $\Phi'_R = (\frac{\partial \Phi}{\partial R})_{z \ll x}$. Here, z is the vertical coordinate of the distance in the cylindrical co-ordinate system and $R = \sqrt{x^2 + z^2}$. The adiabatic sound speed is denoted by a and defined as $a = \sqrt{\gamma P/\rho}$. For simplicity, in the present application, we concentrate only on the inviscid flows for the first study as rigorous investigation of realistic viscous disk is extremely complicated. However, we believe that our basic results presented here would be qualitatively similar to those obtained from viscous flow. In the weak viscosity limit, $W_{x\phi}$ tends to vanish and the angular momentum distribution of the inflowing gas remains conserved along the streamline throughout the disk.

In the weak viscosity limit, we simplify the entropy equation (4) ($Q^+ \to 0$) as:

$$\frac{u}{\gamma - 1}\left[\frac{1}{\rho}\frac{dP}{dx} - \frac{\gamma P}{\rho^2}\frac{d\rho}{dx}\right] = \Lambda, \tag{5}$$

where, the term $\Lambda (= Q^-/\rho h)$ represents the energy lost by the flow. In the present study, we focus on single temperature flow for simplicity and therefore, inclusion of Compton cooling effect is beyond the scope of this work. Moreover, we ignore Bremsstrahlung cooling as it is relatively inefficient process (Chattopadhyay and Chakrabarti 2000). The strength and morphology of magnetic field inside the accretion disk is largely obscured. This propel us to consider the magnetic field to be stochastic in nature. While estimating the strength of the magnetic field, we assume that the magnetic field is in equipartition with the accreting plasma. We introduce a control parameter, (e.g., β), as the ratio of the thermal pressure and the magnetic pressure of the flow which is the measure of equipartition and is given by,

$$\beta = \frac{8\pi \rho k_B T_p}{B^2 \mu m_p}, \tag{6}$$

where, B represents the magnetic field strength, k_B is the Boltzmann constant, μ is the mean molecular weight and m_p is the mass of the proton respectively. In general, the equipartition parameter $\beta \gtrsim 1$ that ensures magnetic fields to remain confined with the accreting plasma (Mandal and Chakrabarti 2005). In addition, we assume an ideal equation of state for accreting gas. The synchrotron emissivity of an electron-proton plasma in a stochastic magnetic field is given by (Shapiro and Teukolsky 1983; Das 2007)

$$\Lambda = \frac{Sa^5}{u}\sqrt{\frac{\Phi'_R}{x^3}}, \tag{7}$$

with

$$S = 15.36 \times 10^{17}\ \frac{\dot{m}\mu^2 e^4}{\beta m_e^3 \gamma^{5/2}} \frac{1}{GM_\odot c^3},$$

where, e and m_e denote charge and mass of electron respectively. We estimate the electron temperature from the expression $T_e = \sqrt{m_e/m_p}T_p$ (Chattopadhyay and Chakrabarti 2002) instead of using the complicated model for electron-ion coupling since such an approach is beyond the present frame work of our paper. The term $\dot{m}$ represents accretion rate in units of Eddington rate that determines the cooling efficiency. In addition, we consider $\gamma = 4/3$, $\beta = 10$ throughout the paper, until otherwise stated.

2.2 Sonic point conditions

As anticipated in the Sect. 1, the accretion solution necessarily meets the transonicity condition in order to satisfy the inner boundary conditions imposed by the event horizon. The general nature of the sonic point can be visualized by solving (1–3) and (5) as,

$$\frac{du}{dx} = \frac{N}{D}, \tag{8}$$

where, the numerator (N) is given by,

$$N = Sa^5\sqrt{\frac{\Phi'_R}{x^3}} - \frac{3u^2a^2}{x(\gamma - 1)} + u^2\frac{(\gamma + 1)}{(\gamma - 1)}\frac{d\Phi_e}{dx} + \frac{u^2a^2}{(\gamma - 1)\Phi'_R}\frac{d\Phi'_R}{dx} \tag{8a}$$

and the denominator (D) is given by,

$$D = \frac{2ua^2}{\gamma - 1} - u^3\frac{(\gamma + 1)}{(\gamma - 1)}. \tag{8b}$$

The first derivative of sound speed is calculated as,

$$\frac{da}{dx}=\left(\frac{a}{u}-\frac{\gamma u}{a}\right)\frac{du}{dx}+\frac{3a}{2x}-\frac{\gamma}{a}\frac{d\Phi_e}{dx}-\frac{a}{2\Phi'_R}\frac{d\Phi'_R}{dx}. \quad (9)$$

In order to obtain a physically acceptable accretion flow solution, the first derivative of radial component of velocity must be finite along the streamline of the flow. Equation (8b) clearly indicates that denominator may vanish at some radius. Since flow is smooth everywhere along the streamline, the point where denominator tends to zero, the numerator must also vanish there. Such a special point where both numerator and denominator vanish simultaneously is known as critical point, or sonic point. At the critical point, we have $N=D=0$. Setting $D=0$ yields the value of Mach number ($M=u/a$) at the sonic points as

$$u_c^2=\frac{2}{(\gamma+1)}a_c^2; \qquad M(x_c)=\sqrt{\frac{2}{(\gamma+1)}}. \quad (10)$$

This expression is exactly same as in (Chakrabarti 1989). This clearly shows that Mach number at the sonic point is not affected by the cooling processes. By using another sonic point condition ($N=0$), we obtain an algebraic equation for sound speed at the sonic point which is given by,

$$S(\gamma-1)\sqrt{\frac{\Phi'_R}{x^3}}a^3+\left(\frac{1}{\Phi'_R}\frac{d\Phi'_R}{dx}-\frac{3}{x}\right)M^2a^2 + (\gamma+1)M^2\frac{d\Phi_e}{dx}=0. \quad (11)$$

Equation (11) enable one to solve for x_c and a_c using a set of flow parameters at the sonic points, namely, $\mathcal{F}=(\mathcal{E}_c,\lambda,\dot{m})$. A global accretion solution whether shocked or shock free, necessarily pass through the sonic point before dives into the black hole. The fact is that a shocked accretion flow must cross the critical point more than once since shock transition in any form must take place from supersonic to sub-sonic branches. Thus the presence of multiple sonic points is necessary for shock transition. The closest and furthest critical point from the black hole horizon correspond to inner and outer critical points. It has been reported that outside the black hole horizon multiple critical points (at most three) exist for a wide range of accretion parameter space (Das 2007 and references therein). A comprehensive study of sonic point properties has already been presented in Chakrabarti (1990), Chakrabarti and Das (2004), and therefore, we will not repeat this.

2.3 Isothermal shock condition

In this paper, our main goal is to explore the thermodynamical properties of isothermal stationary shock waves for cooled accretion flow. In order to obtain a shock induced global accretion solution, sub-sonic flow at the outer edge of the disk smoothly cross the outer sonic points to become super-sonic. In the super-sonic region, flow encounters discontinuous transition in flow variables (i.e., velocity, density, entropy etc.) at the shock location. The isothermal shock jump conditions are explored following the standard fluid dynamical approach. At the shock, high energy post-shock flow jumps into the low energy pre-shock flow. To maintain isothermality condition across the shock, flow efficiently radiated away all the excess energy and entropy through the upper and lower surface of the disk at the shock. Across the shock location mass accretion rate, momentum flux and temperature of the flow remain conserved. In the present work, we ignore the mass loss from the disk. Therefore, various conservation equations across the shock are expressed as:

$$\dot{M}_-=\dot{M}_+; W_-+\Sigma_-u_-^2=W_++\Sigma_+u_+^2; T_-=T_+, \quad (12)$$

where, the subscripts '$-$' and '$+$' denote the quantities just before and after the shock. Here, W represents vertically integrated pressure.

3 Global accretion solutions

A complete global accretion solution is obtained by integrating the dynamical equations (8–9) when the boundary values of energy, angular momentum and accretion rate is known. For a dissipation free environment, energy and angular momentum of the flow continues to be conserved all throughout the disk. This enables one to uniquely determine the location of sonic points. From the sonic point, one can integrate (8–9) inwards up to the horizon and outwards at a large distance to obtain the global solution.

Since synchrotron cooling is incorporated, the specific energy of the accreting matter is not remain conserved along the streamline. As a result, energy of the flow is not a global free parameter now, instead we use it as a local parameter at a given radii. In reality, shock wave joins two independent accretion solutions obtained by using completely different set of flow parameters. One solution passes through the outer sonic point and the other goes through the inner sonic point.

We supply local flow energy to calculate the location of the sonic point by using the sonic point conditions (8a–8b) and the energy equation that are only valid at a given radii and is given by

$$\mathcal{E}(x_c)=\frac{1}{2}u^2(x_c)+na^2(x_c)+\Phi(x_c), \quad (13)$$

where, $\mathcal{E}(x_c)$, $u(x_c)$, $a(x_c)$ and $\Phi(x_c)$ represent the energy, radial velocity, sound speed and the effective potential of the flow at a given sonic radius (x_c). In presence of cooling, we use either inner or outer sonic point as a reference point for

starting the integration for obtaining the flow solution. For a given inner (outer) sonic point, its conjugate outer (inner) sonic point, if it exists, cannot be determined unless a shock is formed as the energy of the flow is not conserved. A detailed description for finding the global shock solutions in a dissipative accretion flow is presented in (Chakrabarti and Das 2004). In this paper, we follow the similar approach to obtain the isothermal shock solution.

3.1 Global shock solution

Figure 1 shows a classic example of complete global solution for a height integrated accretion flow where an isothermal shock waves ties two solutions, one passing through the outer sonic point (O) and the other passing through the inner sonic point (I). The flow motion is depicted by varying Mach number (M) defined as the ratio of radial velocity (u) to the local sound speed (a) with the logarithmic radial distance $\log(x)$ and the direction of the flow motion is indicated by arrows. Matter starts accreting subsonically from the outer edge of the disk (say $x_T = 200$) with energy $\mathcal{E}(x_T) = 1.007$ (including rest mass) and angular momentum $\lambda = 3$ and becomes super-sonic after crossing the outer sonic point at $x_{out} = 67.97$. The specific spin angular momentum of the black hole and the accretion rate are chosen as $a_k = 0.5$ and $\dot{m} = 0.1$ respectively. The width of the shock is considered to be thin across which flow is assumed to be isothermal

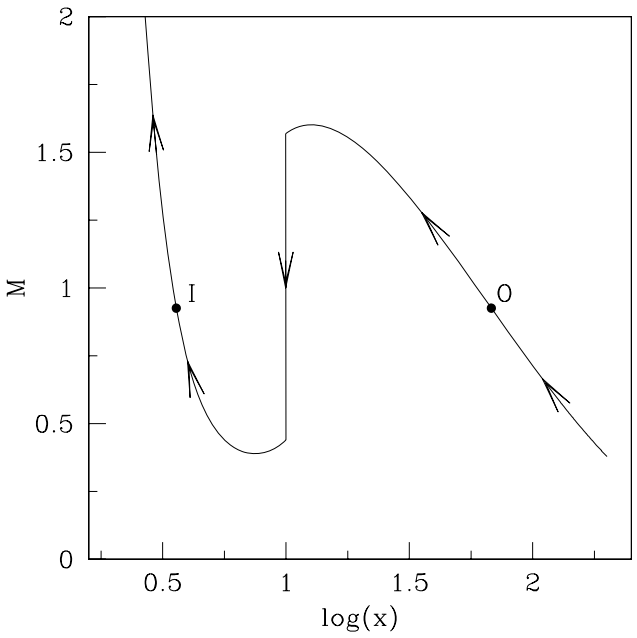

Fig. 1 A classical example of accretion flow solution that transit through the isothermal shock. Mach number ($M = u/a$) of the flow is plotted with logarithmic radial distance. *Arrows* indicate the direction of the flow motion towards the black hole. The *filled circles* marked as O and I represent outer ($x_{out} = 67.97$) and inner ($x_{in} = 3.5885$) sonic points. The arrowed vertical line indicates the location of isothermal shock ($x_s = 9.65$)

in nature. In the super-sonic flow shock conditions are satisfied and a shock is formed at $x_s = 9.65$ denoted by the solid vertical line. Just after the shock transition, flow momentarily slows down and gradually picks up its velocity to become super-sonic in order to satisfy the inner boundary conditions imposed by the black hole after going through the inner sonic point $x_{in} = 3.5885$ denoted by I. At shock, high energy flow ($\mathcal{E}_-$) is connected with the low energy flow ($\mathcal{E}_+$) by releasing the excess energy ($\Delta\mathcal{E} \equiv \mathcal{E}_- - \mathcal{E}_+ = 0.021$) through the upper and lower surface of the shock. These excess energy powers the significant fraction of accreted matter to eject out from the disk as outflows. In addition, since shocks are located in the vicinity of the black hole, such a large amount of energy release could be directly associated with the observed X-ray emission features of AGNs. In the present study, we are not presenting the detail topological behaviour of such accretion flow that may allow isothermal shock transition to avoid repetition (Lu and Yuan 1998).

3.2 General behavior of shock

Now we study how the general properties of isothermal shock waves depend on the flow parameters and the black hole spin. In the left and right panels of Fig. 2, we show the results for $a_k = 0.5$ with prograde flows and $a_k = -0.99$ with retrograde flows, respectively. Upper panels show the variation of shock locations (x_s) with pre-shock energy ($\mathcal{E}_-$) for a set of angular momentum (λ). The flow is assumed to be non-dissipative ($\dot{m} \sim 0$) in the present case. The solid, dashed, dotted and dot-dashed curves correspond to the angular momentum $\lambda = 3.1$, 3.06, 3.02 and 2.98 for $a_k = 0.5$ and $\lambda = 4.4$, 4.3, 4.2 and 4.1 for $a_k = -0.99$ respectively. First notice that for each angular momentum, isothermal shock is formed for wide range of the pre-shock energy ($\mathcal{E}_-$). Similarly, for a given ($\mathcal{E}_-$), isothermal shock exits for a wide range of λ as well. This clearly suggests that isothermal shocks occur in a significant region of parameter space spanned by the pre-shock energy ($\mathcal{E}_-$) and angular momentum (λ) of the flow. For low angular momentum, flow undergoes isothermal shock transition when ($\mathcal{E}_-$) is relatively higher and *vice versa*. A pronounced fact is that for a given set of input parameters ($\mathcal{E}_-, \lambda, a_k, \dot{m}$), there exists a range of pre-shock energy $\mathcal{E}_-^{min} < \mathcal{E}_- < \mathcal{E}_-^{max}$ such that the flow has multiple shocks. One forms closer to the black hole called inner shock (x_{si}) and the other located far away form the black hole referred as outer shock (x_{so}). Now the obvious uncertainty for resolving the multiplicity problem of shock locations is still an open problem. It is however unclear yet which one is actually allowed by nature since both the shocks are found to be stable following the robust stability analysis prescription of (Yang and Kafatos 1995). We find that this uncertainty remains even for a dissipative accretion flow, specially when cooling is effective (see below). Inclusion of more physical processes (e.g., large scale

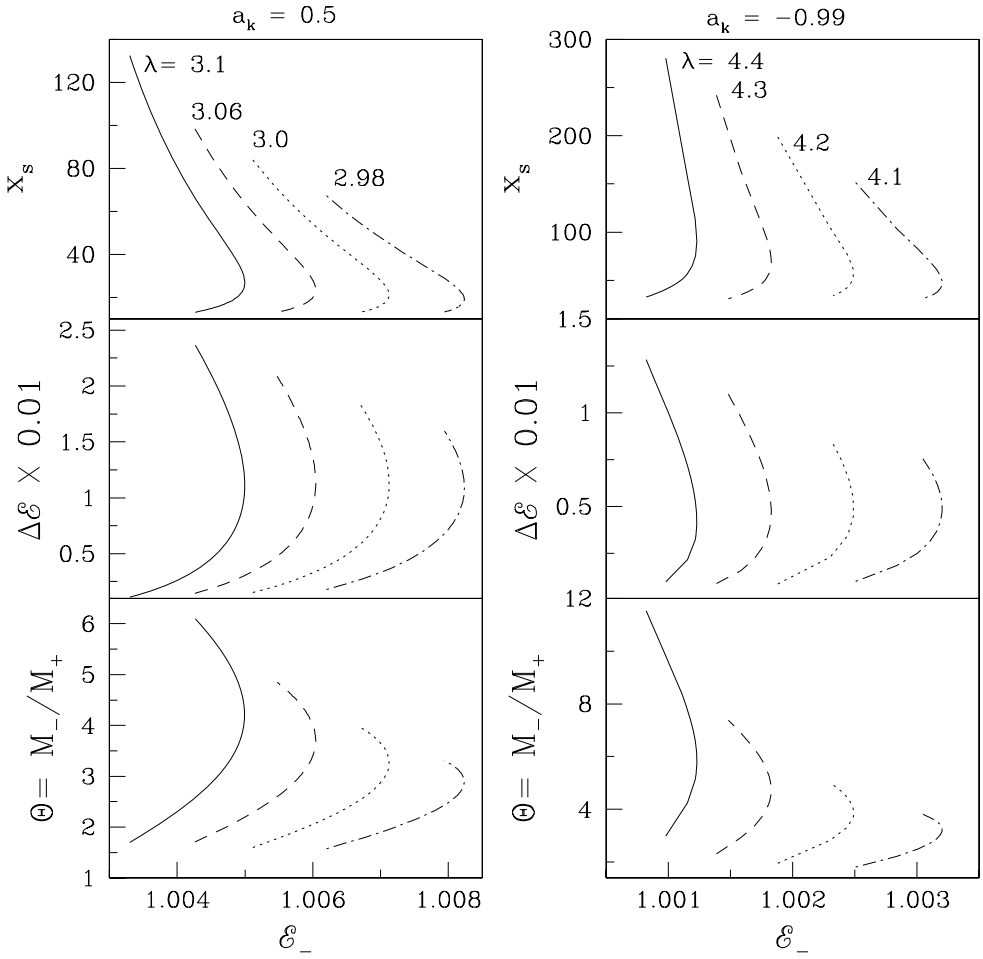

Fig. 2 Variation of flow variables [e.g., shock location (x_s), energy release ($\Delta\mathcal{E}$) and shock strength ($\Theta = M_-/M_+$)] at the isothermal shock location as a function of pre-shock energy for a set of angular momentums (λ). In the *left panel*, *solid*, *dashed*, *dotted* and *dot-dashed curves* are for $\lambda = 3.1, 3.06, 3.2$ and 2.98 in prograde flow with $a_k = 0.5$. In the *right panel*, the same curve styles are followed for $\lambda = 4.4, 4.3, 4.2$ and 4.1 in retrograde flow with $a_k = -0.99$

magnetic field, viscosity, mass loss) may facilitate to identify the unique shock location whose effects we have not included here for simplicity. If $\mathcal{E}_-$ increases further, these two shocks gradually come closer and ultimately merge to a single shock location for a critical pre-shock energy $\mathcal{E}^c_-$. Beyond this energy $\mathcal{E}_- > \mathcal{E}^c_-$ isothermal shock ceases to exits for given angular momentum flow since shock conditions are not favorable there. Of course, the value of critical pre-shock energy ($\mathcal{E}^c_-$) is not universal, but depends on the input parameters ($\lambda, a_k, \dot{m}$).

As we pointed out in the Introduction that isothermal shock connects high energy flow ($\mathcal{E}_-$) to the low energy flow ($\mathcal{E}_+$) by discharging the excess energy ($\Delta\mathcal{E} \equiv \mathcal{E}_- - \mathcal{E}_+$) through the disk surface at the shock. In the middle panel of Fig. 2, we plot the variation of $\Delta\mathcal{E}$ with $\mathcal{E}_-$ for the same set of input parameters as in the upper panels of Fig. 2. A substantial discharge of energy is observed at the shock in all the cases. It is also seen that $\Delta\mathcal{E}$ strongly depends on the flow parameters. An important point is that the amount of energy release at the inner shock location is always larger than the outer one. In addition, prograde flow tends to discharge energy to a greater extent than the retrograde flow. Thus, in the astrophysical context, the implication of the inner shock would be more profound than the outer one.

In the lower panels of Fig. 2, we show the variation of shock strength defined as the ratio between the pre-shock Mach number to the post-shock Mach number with pre-shock energy ($\mathcal{E}_-$) for the same set of input parameter as in upper panel of Fig. 2. It is clear that inner shock is always stronger than the furthest (outer) one. In general, all the above features are very much similar to the results obtained by the (Lu and Yuan 1998). Therefore, we argue that the pseudo-Kerr potential assumed to simulate the geometric effect due to curved space-time around a Kerr black hole is a very useful tool for studying the accretion flow avoiding tedious mathematical complexities.

3.3 Comparison of accretion shock solutions with and without cooling

In order to illustrate the effect of cooling on the dynamical properties of the flow variables, we study the disk structure in absence (solid) and presence (dotted) of cooling for a given set of input parameters at the outer edge of the disk (x_{inj}). As an example, we choose a representative case where

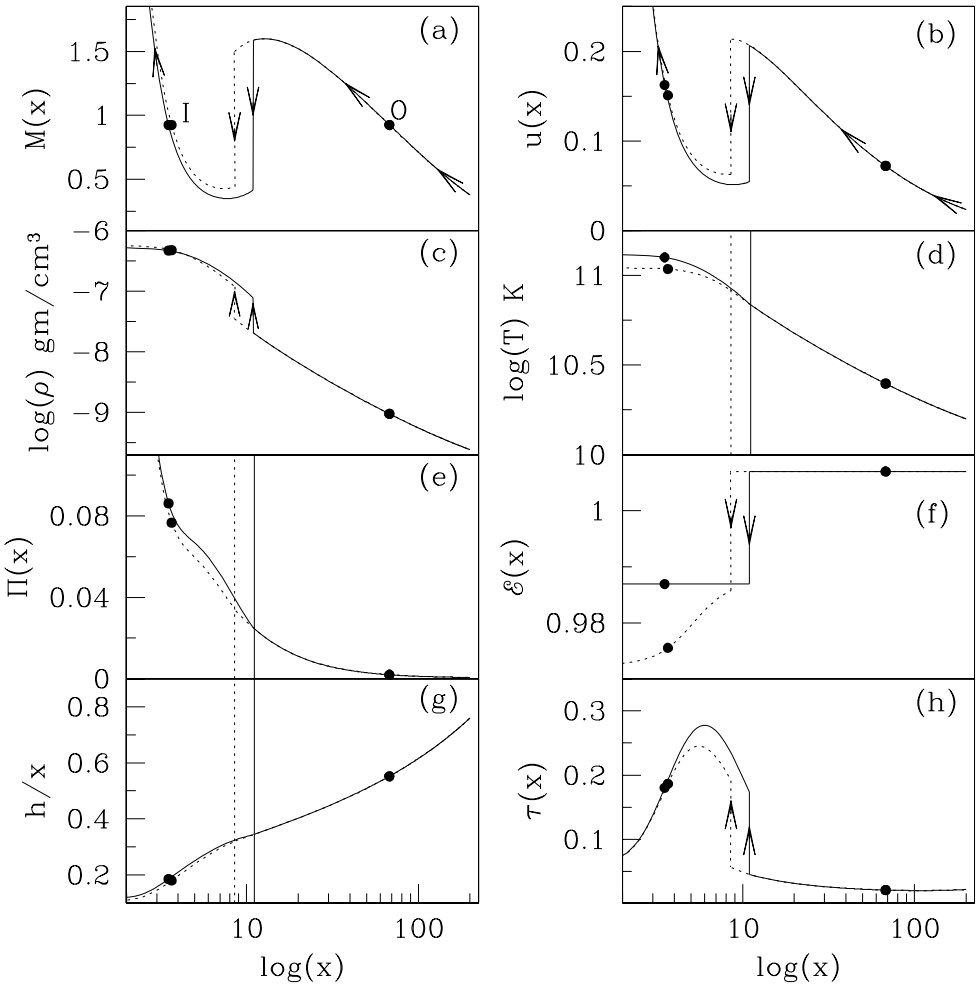

Fig. 3 Accretion solution including inner shock in absence (*solid*) and presence of cooling (*dotted*). Different flow variables are plotted with logarithmic radial distance, (**a**) mach number M, (**b**) radial velocity u, (**c**) logarithmic density $\log(\rho)$, (**d**) logarithmic temperature $\log(T)$, (**e**) total pressure Π, (**f**) energy $\mathcal{E}$, (**g**) aspect ratio h/x and (**h**) scattering optical depth τ in vertical direction. The *filled circle* closer to the black hole horizon is the inner sonic point while the furthest one is the outer sonic point. The *solid* and *dotted vertical lines* denote the isothermal shock location for cooling free and cooled accretion flow. See text for details

both inner and outer shocks are present. In Fig. 3, we demonstrate complete global solutions of a vertically averaged accretion flow that contain inner shock and in Fig. 4, we show the case where outer shock is present. In both the cases, we inject matter subsonically at $x_{inj} = 200$ with local energy $\mathcal{E}(x_{inj}) = 1.007$ and $\lambda = 3.0$. The other input parameters are $\gamma = 4/3$, $a_k = 0.5$. Here, the dissipation free (adiabatic) and dissipative flows are characterize by $\dot{m} \sim 0$ and $\dot{m} = 0.25$ respectively.

Each panel depicts the variation of flow variable with logarithmic radial distance. In Figs. 3a and 4a, we plot the Mach number ($M = u/a$) variation of the accreting flow. Sub-sonic flow first crosses the outer sonic point (O) to become super-sonic. The isothermal shock conditions are satisfied in the super-sonic flow at two different locations for cooling free flow and the discontinuous transitions of flow variables are observed at $x_s = 10.93$ (inner shock) and 27.45 (outer shock) denoted by the solid vertical line in Figs. 3a and 4a respectively. The arrows indicate the direction of the flow motion during accretion towards the black hole. As cooling is turn on ($\dot{m} = 0.25$), the inner shock front moves forward ($x_s = 8.52$) and the outer shock moves backward ($x_s = 54.06$) as depicted by the dotted vertical lines in Figs. 3a–4a. This distinctly reveals that multiple shock locations still persist in a cooled accretion flow and the dynamics of the inner and outer shock respond to synchrotron cooling in a completely opposite manner. For clarity purpose, we only present four representative shock solutions. In reality, flow may suffer shock transition at any radius between outer and inner most radius depending on the accretion rate ($\dot{m}$). In Figs. 3b–4b, we plot the variation of radial velocity (u) as a function of logarithmic radial distance for adiabatic and cooling induced flow solution using same set of input parameters as in Figs. 3a–4a. We demonstrate the density profile for cooling free and cooled flow in Figs. 3c–4c. In all the cases, density jumps at the shock location. This mainly because of the reduction of radial velocity across the shock. Adiabatic flow feels less compression at the outer shock location compared to the inner shock location as velocity jump is relatively small there. Thus, strength of the inner shock is always higher than the outer shock. Similar behaviour is seen to continue even in presence of cooling. Overall, the post-shock density profile is relatively weaker in a cooled flow primarily due to the high post-shock velocity

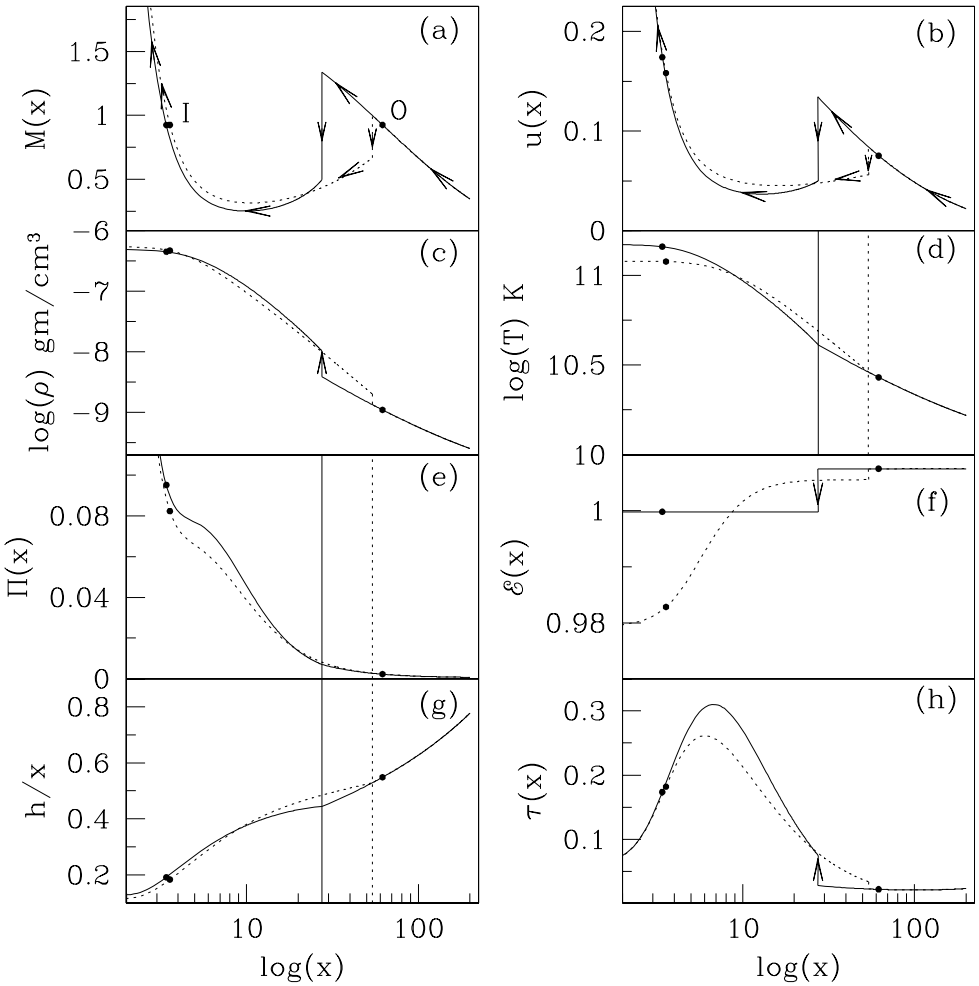

Fig. 4 Same as Fig. 3, but for outer shock case. See text for details

compared to the adiabatic flow. The geometric compression in the disk causes the rise of flow temperature as it accrets inward although flow maintains uniform temperature distribution across the shock to preserve isothermality conditions. That is demonstrated in Figs. 3d–4d. The dotted and solid vertical lines denote the location of shocks in both cooling and cooling free cases. In the pre-shock flow, the effect of cooling is not significant as density and temperature are very low. On the contrary, density raises catastrophically at the shock that enhances cooling efficiency causing the decrease of flow temperature at the inner part of the disk as observed in the figures. Since $a \propto \sqrt{T}$, sound speed also follows similar radial dependence as temperature. In Figs. 3e–4e, we plot the total pressure (thermal + ram). It is observed that pressure balance condition holds in all cases across the shock which is essential to hold standing shock. As we pointed out earlier that energy of flow undergoes a discontinuous jump at the shock. In Figs. 3f–4f, we show the variation of energy with $\log(x)$ where the solid and dotted vertical lines with arrows indicate the shock locations. One of the noticeable features is that energy release at the inner shock is much higher than that at the outer shock location. Similar situation is maintained even for a cooled accretion flow. In presence of cooling, as flow loses energy when it accrets, there is a certain possibility to obtain a shock solution for very low energy flow at the inner part of the disk although this flow may not participate in shock solution when cooling is absent. Thus, cooling may allow one to get shock solution with very low energy flow. The most encouraging fact is that the line emissions from AGNs are thought to be originated from a cooled accretion disk having a source of high energy radiation above the disk equatorial plane. These lines are frequently exhibits broadening characteristic (Nandra and Pounds 1994) as they arise from the region close to the central engine (Fabian et al. 1989), a similar place of inner shock location. All these observational arguments clearly indicates that isothermal shock solution perhaps would be a very good choice to explain AGN sources. On the top of that inner shock would be more favorable in terms of energetics. In Figs. 3g–4g, we plot the dependence of vertical scale-height to the radius. Figures clearly shows that post-shock flow generally leads to the geometrically thin disk all its way to the horizon. The accretion rate equation indicates that density profile in the post-shock flow would be steeper

due to simultaneous decrease of radial velocity and vertical scale-height. This makes the post-shock flow significantly opaque to the emitted photons although it remains optically thin ($\tau < 1$). This is shown in Figs. 3h–4h. Interestingly, cooling dominated flow is more optically thin than the adiabatic flow irrespective to the shock location. This eventually suggests that the possibility of escaping hard photons through the surface of the disk is higher for a cooled accretion flow.

3.4 Shock dynamics and shock properties

So far, we have only studied the shocked accretion disk structure of a flow injected from a fixed outer edge of the disk with a given local energy and angular momentum. In the next, we wish to continue our study to explore the dependence of shock properties on angular momentum and energy of the flow. As before, we study both inner (x_{si}) and outer (x_{so}) shock properties simultaneously.

In Fig. 5, we compare the shock properties as a function of accretion rate ($\dot{m}$) for a set of angular momentums. In all cases, flow is injected at the outer edge of the disk $x_{inj} = 200$ with local energy $\mathcal{E}_{inj} = 1.0065$. We present the results of inner and outer shocks in the left and right panels of Fig. 5. In the left panel, solid, dashed and dotted curves are for $\lambda = 3, 3.01$ and 3.02 and in the right panel, the same curve styles stand for $\lambda = 3.0, 3.02$ and 3.04, respectively. The other input parameters are $\gamma = 4/3$ and $a_k = 0.5$. Figure 5a–b show that stationary inner (x_{si}) and outer (x_{so}) shocks exist for a wide range of accretion rate. However, the range of isothermal shock locations (x_{si} and/or x_{so}) tends to become narrower in a cooled flow as λ decreases for a given local energy $\mathcal{E}_{inj}$ at the injection point. For given angular momentum λ, x_{si} moves inward while x_{so} moves outward with the enhancement of accretion rate. Beyond a critical accretion rate limit ($\dot{m} > \dot{m}^c_{xs}$), standing shocks disappear as isothermal shock conditions are not satisfied there. This naturally introduce a fact that the possibility of isothermal shock formation is likely to be reduced with the raise of accretion rate. Obviously, the critical accretion rate limit largely depends on the inflow parameters and black hole spin $\dot{m}_{cs}(\lambda, \mathcal{E}, a_k)$. However, non-steady shock still may exist although the study such scenarios are beyond the scope of this paper. What is more, for a given accretion rate, x_{si} develops at larger radii while x_{so} settles down at closer radii when angular momentum of the flow is increased.

We already pointed out that at the location of isothermal shock accretion flow discharge a significant fraction of its energy that may powered the escaped relativistic particles

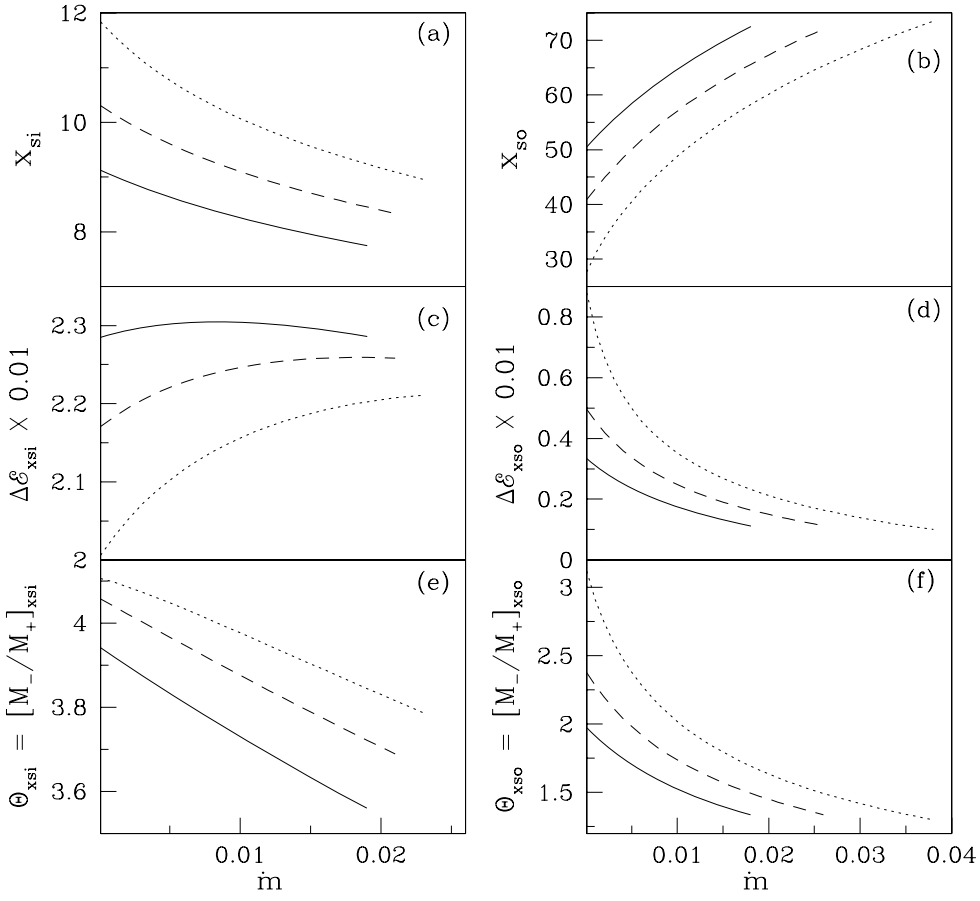

Fig. 5 (**a**–**b**) Variation of inner (*left panel*) and outer (*right panel*) shock locations with accretion rate. Flows are injected at the outer edge of the disk with same energy and angular momentum. In the *left panel*, *solid*, *dashed* and *dotted curves* are for $\lambda = 3, 3.01$ and 3.02 while in the right the same curve types are used for $\lambda = 3, 3.02$ and 3.04 respectively. (**c**–**d**) Variation of amount of energy release ($\Delta\mathcal{E}$) with accretion rate for the same set of parameters as in (**a**–**b**). (**e**–**f**) Variation of shock strength (Θ) with accretion rate for the same set of parameters as in (**a**–**b**). In all cases, energy at the outer edge is $\mathcal{E}_{inj} = 1.0065$ and specific spin angular momentum is $a_k = 0.5$

as relativistic outflows and could be responsible for explaining the AGN spectra. Thus it is very useful to study the dependencies of energy loss across the isothermal shock on the accretion flow parameters. In Fig. 5c–d, we plot how the amount of energy loss at the inner shock location ($\Delta\mathcal{E}_{xci}$) and outer shock location ($\Delta\mathcal{E}_{xco}$) varies with accretion rate ($\dot{m}$). Here, we use the same set of initial parameters as in Fig. 5a–b. We find that for a given angular momentum flow, $\Delta\mathcal{E}_{xci}$ shows strong correlation whereas $\Delta\mathcal{E}_{xco}$ exhibits anti-correlation with the accretion rate $\dot{m}$. We find that energy discharge at the inner shock is order of magnitude higher than the outer shock location. Another important features to note regarding the angular momentum dependence is that $\Delta\mathcal{E}_{xci}$ is always larger for low λ while a completely opposite features is observed in case of $\Delta\mathcal{E}_{xco}$. The most important things to reveal in this regard is that $\Delta\mathcal{E}$ primarily depends on the shock location for flows with a given combination of input parameters. When isothermal shocks (x_{ci} and x_{co}) forms closer to the black hole, $\Delta\mathcal{E}$ increases. This is quite evident because the gravitational potential energy to be discharged is larger when shocks form close to the black hole event horizon.

In our further study of shock properties, we compute the variation of shock strength (Θ) with accretion rate. In case of isothermal shock, shock strength identically matches with the compression ratio which usually measures the amount of density compression across the shock and is defined as the ratio of the vertically averaged post-shock density to the pre-shock density. In Fig. 5e–f, we draw the variation of shock strength (Θ_{xci} and Θ_{xco}) calculated at inner and outer shock location respectively with accretion rate using the same set of input parameters as in Fig. 5a–b. It is observed that strength of the shock generally anti-correlates with accretion rate for a fixed λ. On the contrary, a correlation is found between shock strength and λ when accretion rate is fixed. There is a cut-off at a critical accretion rate limit in both inner and outer shock cases as shock conditions are not fulfilled there.

In order to understand the energy dependence of an isothermal shocked accretion flow, we present, in Fig. 6, the variation of inner and outer shock properties (as in Fig. 5. e.g., shock location, energy release at the shock and shock strength) with accretion rate for flows with different energies. As in the earlier case, the inner and outer shock properties are displayed in the left and right panels respectively. Solid, dashed and dotted curve in the left panel is for $\mathcal{E}_{inj} = 1.007$, 1.00725 and 1.0075 and the same curve style is used in the right panel for $\mathcal{E}_{inj} = 1.006$, 1.0065 and 1.007, respectively. The corresponding angular momentum in left and right panels are chosen as $\lambda = 3.0$ and 3.02 respectively.

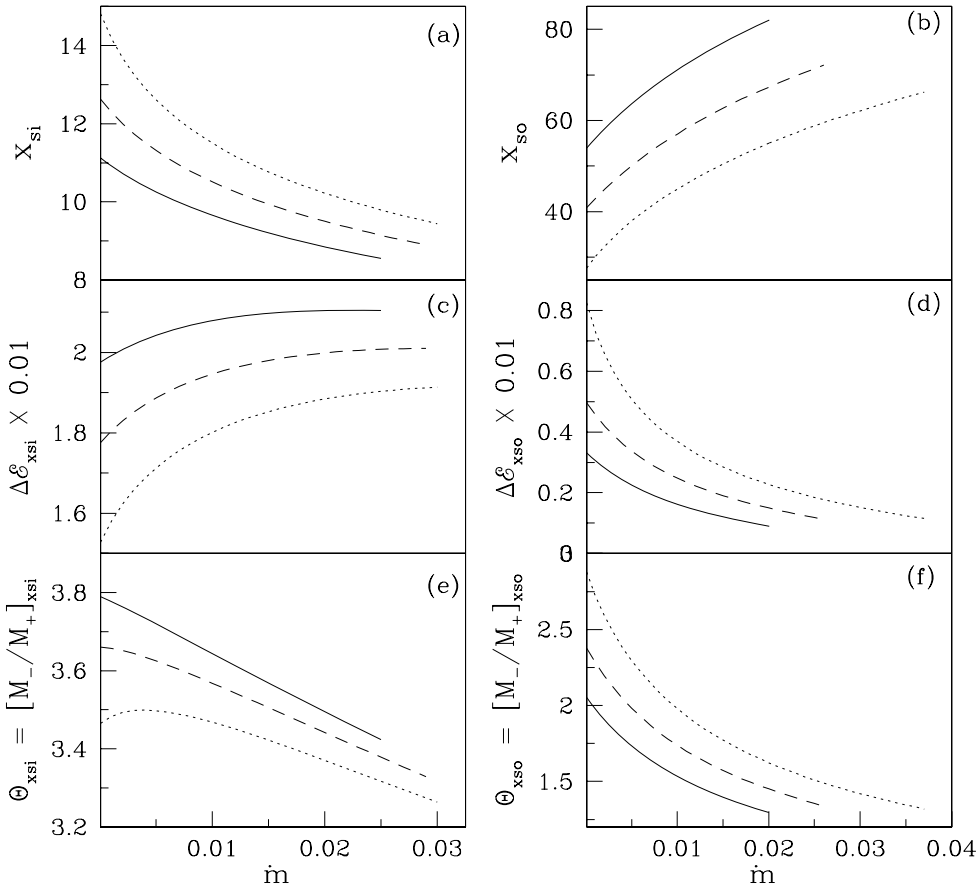

Fig. 6 Same as Fig. 5 except angular momentum is kept fixed at the outer edge and energy is varied. In the *left panel*, *solid dashed* and *dotted curves* are for $\mathcal{E}_{inj} = 1.007$, 1.00725 and 1.0075 respectively. Angular momentum at the injection point is $\lambda_{inj} = 3.0$. In the *right panel*, *solid dashed* and *dotted curves* are for $\mathcal{E}_{inj} = 1.006$, 1.0065 and 1.007 respectively. Angular momentum at the injection point is $\lambda_{inj} = 3.02$. In all cases, specific spin angular momentum is chosen as $a_k = 0.5$

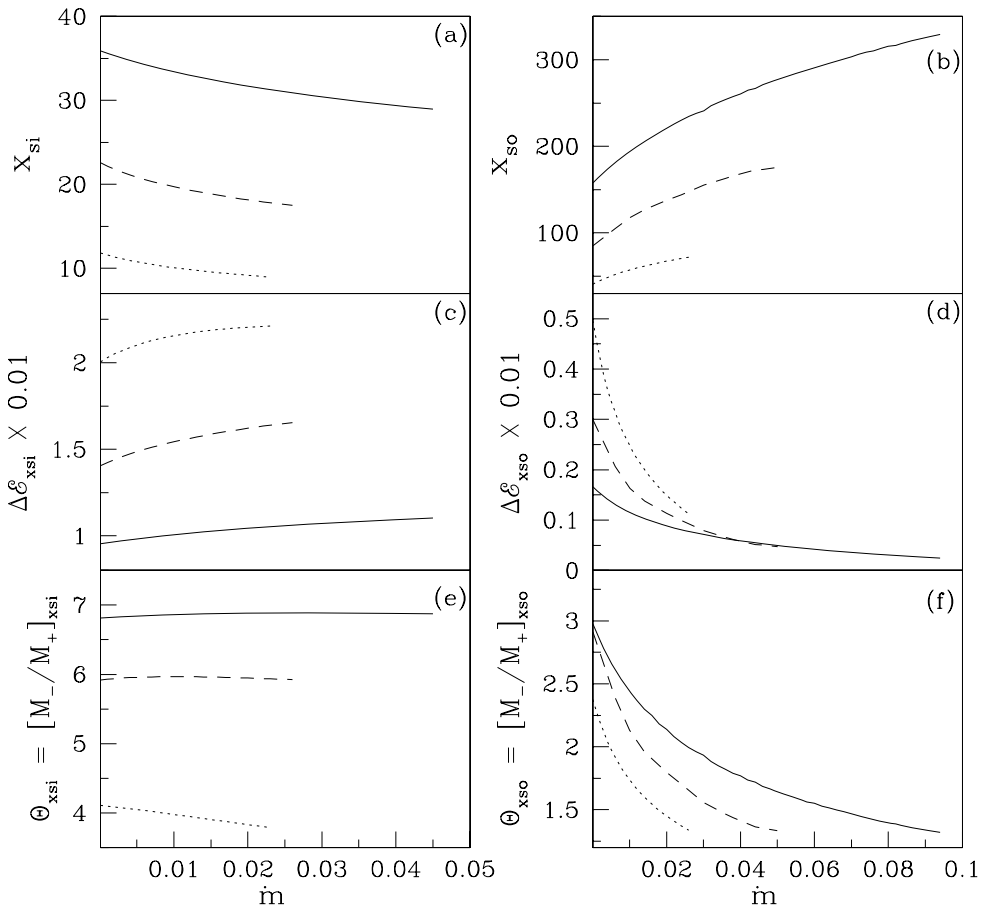

Fig. 7 Same as Fig. 5, but specific spin angular momentum of the black hole is varied. *Solid*, *dashed* and *dotted curves* are for $(\mathcal{E}_{inj}, \lambda_{inj}, a_k) = (1.0016, 4.3, -0.99)$, $(1.0029, 3.6, 0.0)$ and $(1.0065, 3.02, 0.5)$ respectively. See text for details

The qualitative variation of shock properties very much similar to the case presented in Fig. 5a–f. It is realized that, for a fixed accretion rate, x_{ci} forms at further radii while x_{co} develops at closer distance when energy of the accreting flow is higher. Another noticeable feature is that the amount of energy release ($\Delta\mathcal{E}_{xci/xco}$) at the shock mainly depends on the shock location for a set of input parameters as pointed out in Fig. 5. If shock forms closer to the black hole, $\Delta\mathcal{E}_{xci/xco}$ increases with any given combination of input parameters that may allow shock transitions. These behaviour is certainly witnessed again form Fig. 6c–d. In Fig. 6e–f, we draw the variation of shock strength ($\Theta_{xci/xco}$) for the same set of parameters as used in Fig. 6a–b. In general, shock strength decreases with the increase of accretion rate although there is tendency to increase Θ at inner shock for higher energy flow. In all the cases, there exists a cut-off at critical accretion rate limit above which isothermal shocks do not exists (isothermal shock conditions are not meet).

As we discussed above, the general features of shock properties is strongly depends on the energy and the angular momentum of the flow. Overall, cooling plays a crucial role in deciding the shock formation, energy release at the shock and shock strength. More importantly, x_{ci} and x_{co} shows a completely opposite response to cooling as far as the shock dynamics and energy discharge at the shock is concerned. Since cooling acts as a dissipation process in the flow, the possibility of isothermal shock formation is reduced with the increment of cooling rate. We will discuss this in Sect. 4.

For the sake of completeness, in Fig. 7, we demonstrate the dependence of shock properties on the spin angular momentum of the black hole a_k for a range of accretion rate $\dot{m}$. As before, left panel is for inner shock and the right panel is for outer shock. Here, we present the results for prograde ($a_k > 0$) as well as retrograde flow ($a_k < 0$). In all the cases, matter is injected at the outer edge of the disk $x_{inj} = 200$. The input parameters $(\mathcal{E}_{inj}, \lambda, a_k)$ correspond to solid, dashed and dotted are $(1.0016, 4.3, -0.99)$, $(1.0029, 3.6, 0.0)$ and $(1.0065, 3.02, 0.5)$ respectively. We find that isothermal shock transition is allowed around a stationary (Schwarzschild) black hole, rotating black hole with prograde flow and rotating flow with retrograde flow. In particular, isothermal shocks exist in all cases for a large range accretion rate $\dot{m}$. In the upper panels of Fig. 7, we show the variation of shock locations (x_{si}, x_{so}) with accretion rate $\dot{m}$. As cooling increased, x_{si} tends to shift inward while x_{so} recedes further away from the black hole. An important feature is seen in the middle panel of Fig. 7

where it is evident that around a rotating black hole prograde flow is more efficient to disperse its energy compared to the retrograde flow at the isothermal shock location. It is perhaps due to the manifestation of frame dragging effect, as rotating black hole assists prograde flow to gain its motion during accretion and therefore, more energy is expected to release at the shock. The situation is completely opposite for retrograde flow as rotating black hole tends to redirect the flow motion in its favor causing the least energy discharge. Similar to Figs. 5–6, here we also notice that energy release at the shock strongly depends on the accretion rate. In the lower panels of Fig. 7 we plot the variation of the shock strength with accretion rate $\dot{m}$ for same set of parameters as used in upper panels of Fig. 7. We find that, strong shocks are formed in the inner part of the disk whereas outer shocks are relatively weaker. Notice that Θ_{xsi} feebly depends on the accretion rate while Θ_{xsi} gradually decreases as the accretion rate is enhanced.

4 Parameter space for isothermal shock

In Sect. 3, we have seen that the global shock induced accretion solutions are not isolated solutions and they exist for a wide range of energies and angular momenta. In this section, we wish to interpret the effects of cooling on the properties of shock included dissipative accretion flow. While doing this, we classify the parameter space spanned by the specific angular momentum (λ) and specific energy of the flow at the inner sonic point ($\mathcal{E}_{in}$) as a function of accretion rate. In Fig. 8, we draw the boundary of the parameter space that allows standing isothermal shock transition in accretion flow. The solid boundary shows the effective region of parameter space for shock (inner and/or outer) for non-dissipative flow. We choose $a_k = 0.5$ and $\gamma = 4/3$. As anticipated earlier, we observe that parameter space for standing isothermal shock is severely affected by the cooling effect. We identify the modified region of parameter space for stationary isothermal shock in terms of cooling efficiency ($\dot{m}$). The region bounded by dashed, dotted and dot-dashed curves are for $\dot{m} = 0.025, 0.1$ and 0.2, respectively. At higher accretion rate, the effective region of parameter space is shrunk and shifted to the low energy region. This is significant as cooling allows low energy flow passing through the inner sonic point to participate in shock transition. As accretion rate is increased beyond a critical limit ($\dot{m} > \dot{m}_{cs}$), parameter space disappears completely. This critical accretion rate greatly depends on the other inflow parameters. Thus, isothermal shock can only possible for a given range of input parameters ($\mathcal{E}_{in}, \lambda, a_k, \dot{m}$).

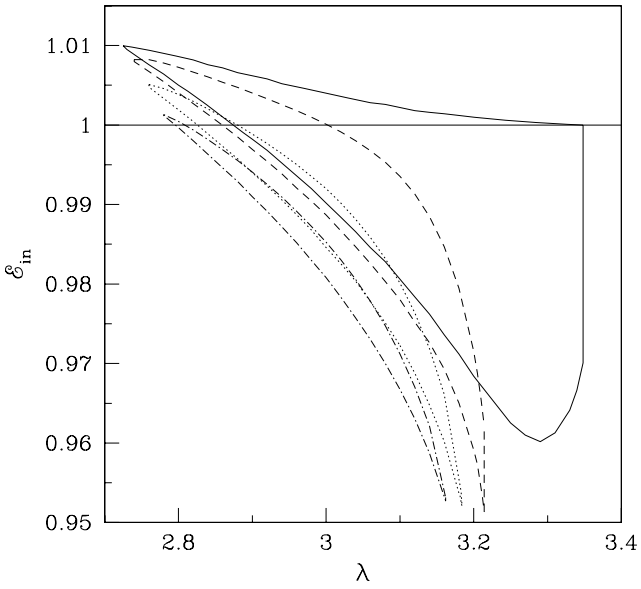

Fig. 8 Classification of parameter space for standing isothermal shock as a function of accretion rate. The region bounded by solid curve is for cooling free flow and the region bounded by *dashed*, *dotted* and *dot-dashed curves* are for flows with $\dot{m} = 0.025, 0.1$ and 0.2, respectively. Specific spin angular momentum of the black hole is chosen as $a_k = 0.5$

5 Concluding remarks

In the present paper, we described the formalism for studying the dynamical structure of an isothermal shock included polytropic accretion flow in presence of cooling. We primarily consider synchrotron cooling which has a profound effect on the dynamical structure of the accretion flow as well as the observed radiation properties. The importance of isothermal shock is being first discussed by (Chakrabarti and Abramowicz 1990) since huge amount of energy release is expected at the location of isothermal shock. In the past, the properties of isothermal shock wave was studied either for adiabatic flow considering full general relativity (Lu and Yuan 1998; Fukumura and Tsuruta 2004) or for isothermal flow using various Pseudo-potentials for Schwarzschild black hole (Das et al. 2003). In all these work, it was reported that isothermal shock location could be treated as a natural site for possible radiation sources that may be responsible to power the observed X-ray flares (strong). However, no attempts have been made to study the complete isothermal shock induced accretion solution in presence of synchrotron cooling although cooling may imposed significant impact on the dynamical structure as well as emission properties from the disk. In this work, we obtain a complete global shocked accretion solution for a wide range of accretion rate. We also provided the dependence of hydrodynamical and thermodynamical flow properties at shock on the various accretion parameters.

We have shown that the multiplicity of the isothermal shock locations continues to present for an accretion flow in presence of cooling. For higher cooling, inner shock location tends to move towards the black hole whereas the outer shock recedes outwards. Thus, the response of cooling in outer and inner shock location is completely opposite. In general, energy release at the inner shock location is higher than the outer shock that clearly provides a hint that inner shock location is more favorable in terms of energetics. Moreover, the amount of energy release at the inner shock location gradually increases while it decreases at the outer shock with the increase of accretion rate.

We identify the effective region of parameter space that allows stationary isothermal shock waves as a function of accretion rate. We observe that boundary of the parameter space contracts when accretion rate is increased. In other words, cooling reduces the possibility of shock formation. When cooling is above its critical value, stationary isothermal shock ceases to exit as the shock conditions are not satisfied there. However, non-steady shocks still may present as accretion flow possesses multiple sonic points (Ryu et al. 1997). Overall, cooling significantly alter the flow characteristics as well as parameter space for stationary isothermal shock.

We wish to address another important findings of our work here. Although we incorporated cooling mechanism in our present study, a substantial amount of energy discharge is observed from the isothermal shock location just to maintain isothermality across the shock front. This huge excess energy ($\sim 2 \times 10^{18}$ erg g^{-1}) may be exhausted as a radiation source of strong X-ray flare. Another possibility is to drive a part of the accreted matter as relativistic outflows (Le and Becker 2005). All such theoretical interpretations have observational support as it was recently reported that both X-ray flares and the outflows are originated from the vicinity of the black hole (Junor et al. 1999; Biretta et al. 2002; Falcke 1999). The typical size of the post-shock flow which possibly responsible for various diverse phenomenon is reasonably coherent with the observational results (Yuan et al. 2006).

In this work, we use pseudo-Kerr potential introduced by (Mondal and Chakrabarti 2006) that successfully describe the similar space time geometry around a Kerr black hole as far as the transonic properties of the flow is concerned. The approximation of pseudo-Kerr potential allows us to study the non-linear polytropic accretion flow solution including shock in a simpler way. At present, it is beyond the scope of this paper to compare our solutions with the exact general relativistic results although we were able to reproduce the similar results in the adiabatic limit as in (Lu and Yuan 1998). Therefore, we argue that our solutions would still provide qualitatively similar results as of general relativistic calculations for $a_k < 0.8$.

In our current approach, we study the vertically averaged thin accretion disk model without considering the disk-jet system together. In reality, outflows/jets may be originated from the inner part of the disk, specially at the location of isothermal shock as it behaves like a energy reservoir. Once outflows/jets are generated, the post-shock pressure necessarily gets reduced causing the stationary shock to move inward as to maintain pressure balance across it. This clearly points out that the dynamical structure of the disk will definitely be modified in a realistic coupled accretion-ejection system. We plan to consider this as a future work and will be reported elsewhere.

References

Abramowicz, M.A., Czerny, B., Lasota, J.P., Szuszkiewicz, E.: Slim accretion disks. Astrophys. J. **332**, 646 (1988)

Becker, P.A., Le, T.: Inner boundary conditions for advection-dominated accretion onto black holes. Astrophys. J. **588**, 408 (2003)

Biretta, J.A., Junor, W., Livio, M.: Evidence for initial jet formation by an accretion disk in the radio galaxy M87. NewA Rev **46**, 239 (2002)

Chakrabarti, S.K.: Standing Rankine-Hugoniot shocks in the hybrid model flows of the black hole accretion and winds. Astrophys. J. **347**, 365 (1989)

Chakrabarti, S.K.: Theory of Transonic Astrophysical Flows. World Scientific Publishing, Singapore (1990)

Chakrabarti, S.K.: Global solutions of viscous transonic flows in Kerr geometry—I. Weak viscosity limit. Mon. Not. R. Astron. Soc. **283**, 325 (1996a)

Chakrabarti, S.K.: Grand unification of solutions of accretion and winds around black holes and neutron stars. Astrophys. J. **464**, 664 (1996b)

Chakrabarti, S.K.: Estimation and effects of the mass outflow from shock compressed flow around compact objects. Astron. Astrophys. **351**, 185 (1999)

Chakrabarti, S.K., Abramowicz, M.: Standing shocks in adiabatic black hole accretion of rotating matter. Astrophys. J. **350**, 281 (1990)

Chakrabarti, S.K., Das, S.: Properties of accretion shock waves in viscous flows around black holes. Mon. Not. R. Astron. Soc. **349**, 649 (2004)

Chakrabarti, S.K., Mandal, S.: The spectral properties of shocked two-component accretion flows in the presence of synchrotron emission. Astrophys. J. **642**, 49 (2006)

Chakrabarti, S.K., Molteni, D.: Smoothed particle hydrodynamics confronts theory: formation of standing shocks in accretion disks and winds around black holes. Astrophys. J. **417**, 671 (1993)

Chakrabarti, S.K., Titarchuk, L.G.: Spectral properties of accretion disks around galactic and extragalactic black holes. Astrophys. J. **455**, 623 (1995)

Chattopadhyay, I., Chakrabarti, S.K.: A comparative study of bondi-type and radiative outflows around compact objects. Int. J. Mod. Phys. D **9**, 717 (2000)

Chattopadhyay, I., Chakrabarti, S.K.: Radiatively driven plasma jets around compact objects. Mon. Not. R. Astron. Soc. **333**, 454 (2002)

Chattopadhyay, I., Das, S.: Mass loss from viscous advective disc. NewA **12**, 454 (2007)

Das, S.: Behaviour of dissipative accretion flows around black holes. Mon. Not. R. Astron. Soc. **376**, 1659 (2007)

Das, S., Chakrabarti, S.K.: Parameter space study of the magnetohydrodynamic accretion flows around compact objects. Mon. Not. R. Astron. Soc. **374**, 729 (2007)

Das, S., Chattopadhyay, I.: Computation of mass loss from viscous accretion disc in presence of cooling. NewA **13**, 549 (2008)

Das, S., Chattopadhyay, I., Chakrabarti, S.K.: Standing shocks around black holes: an analytical study. Astrophys. J. **557**, 983 (2001a)

Das, S., Chattopadhyay, I., Nandi, A., Chakrabarti, S.K.: Computation of outflow rates from accretion disks around black holes. Astron. Astrophys. **379**, 683 (2001b)

Das, T.K., Pendharkar, J.K., Mitra, S.: Multitransonic black hole accretion disks with isothermal standing shocks. Astrophys. J. **592**, 1078 (2003)

Fabian, A.C., Rees, M., Stella, L., White, N.E.: X-ray fluorescence from the inner disc in Cygnus X-1. Mon. Not. R. Astron. Soc. **238**, 729 (1989)

Falcke, H.: The jet model for SGR A*. Astron. Soc. Pac. Conf. Ser. **186**, 148 (1999)

Fukue, J.: Transonic disk accretion revisited. Publ. Astron. Soc. Jpn. **39**, 309 (1987)

Fukumura, K., Kazanas, D.: Accretion disk illumination in Schwarzschild and Kerr geometries: fitting formulae. Astrophys. J. **664**, 14 (2007)

Fukumura, K., Tsuruta, S.: Isothermal shock formation in nonequatorial accretion flows around Kerr black holes. Astrophys. J. **611**, 964 (2004)

Hameury, J.M., Lasota, J.P., McClintock, J.E., Narayan, R.: Advection-dominated flows around black holes and the X-ray delay in the outburst of GRO J1655-40. Astrophys. J. **489**, 234 (1997)

Hawley, J.F., Smarr, L.L., Wilson, J.R.: A numerical study of nonspherical black hole accretion. I—Equations and test problems. Astrophys. J. **277**, 296 (1984a)

Hawley, J.F., Smarr, L.L., Wilson, J.R.: A numerical study of nonspherical black hole accretion. II—Finite differencing and code calibration. Astrophys. J. Suppl. Ser. **55**, 211 (1984b)

Junor, W., Biretta, J.A., Livio, M.: Formation of the radio jet in M87 at 100 Schwarzschild radii from the central black hole. Nature **401**, 891 (1999)

Le, T., Becker, P.A.: Particle acceleration and the production of relativistic outflows in advection-dominated accretion disks with shocks. Astrophys. J. **632**, 476 (2005)

Lu, J.F., Yuan, F.: Global solutions of adiabatic accretion flows with isothermal shocks in Kerr black hole geometry. Mon. Not. R. Astron. Soc. **295**, 66 (1998)

Mandal, S., Chakrabarti, S.K.: Accretion shock signatures in the spectrum of two-temperature advective flows around black holes. Astron. Astrophys. **434**, 839 (2005)

Manmoto, T.: Advection-dominated accretion flow around a Kerr black hole. Astrophys. J. **534**, 734 (2000)

Matsumoto, R., Kato, S., Fukue, J., Okazaki, A.T.: Viscous transonic flow around the inner edge of geometrically thin accretion disks. Publ. Astron. Soc. Jpn. **36**, 7 (1984)

Miller, J.M.: 2007: Relativistic X-Ray lines from the inner accretion disks around black holes. Ann. Rev. Astron. Astrophys. **45**, 441 (2007)

Mondal, S., Chakrabarti, S.K.: Studies of accretion flows around rotating black holes—II. Standing shocks in the pseudo-Kerr geometry. Mon. Not. R. Astron. Soc. **371**, 1418 (2006)

Nandra, K., Pounds, K.A.: GINGA observations of the X-ray spectra of Seyfert Galaxies. Mon. Not. R. Astron. Soc. **268**, 405 (1994)

Narayan, R., Yi, I.: Advection-dominated accretion: a self-similar solution. Astrophys. J. Lett. **428**, 13 (1994)

Shapiro, S.L., Teukolsky, S.A.: Black Holes, White Dwarfs and Neutron Stars: The Physics of Compact Objects. Wiley-Interscience Publication, New York (1983)

Ryu, D., Chakrabarti, S.K., Molteni, D.: Zero-energy rotating accretion flows near a black hole. Astrophys. J. **474**, 378 (1997)

Yang, R., Kafatos, M.: Shock study in fully relativistic isothermal flows II. Astron. Astrophys. **295**, 238 (1995)

Yuan, F., Shen, Z.-Q., Huang, L.: Testing the radiatively inefficient accretion flow model for Sagittarius A* using the size measurements. Astrophys. J. **642**, 45 (2006)